A general metadynamics protocol to simulate activation/deactivation of Class A GPCRs: proof of principle for the serotonin receptor

Jacqueline C. Calderón,^a Passainte Ibrahim,^b Dorothea Gobbo,^{c,d} Francesco Luigi Gervasio^{c,d,e} and Timothy Clark.^a

^a Computer-Chemistry-Center, Department of Chemistry and Pharmacy, Friedrich-Alexander-University Erlangen-Nuernberg, Naegelsbachstr. 25, 91052 Erlangen, Germany.

^b Institute of Medical Physics and Biophysics, Faculty of Medicine, University of Leipzig, Germany.

^c Pharmaceutical Sciences, University of Geneva, CH1206, Geneva, Switzerland.

^d Institute of Pharmaceutical Sciences of Western Switzerland, CH1206 Geneva, Switzerland.

^e Chemistry Department, University College London, WC1H 0AJ London, UK.

* Timothy Clark & Francesco Luigi Gervasio.

Email: <u>Tim.Clark@fau.de</u>; <u>Francesco.Gervasio@unige.ch</u>

Molecular Dynamics; Metadynamics; Activation Free-Energy Profile; G-Protein Coupled Receptor; 5-HT_{1A}.

ABSTRACT

We present a generally applicable metadynamics protocol for characterizing the activation freeenergy profiles of class A G-protein coupled receptors (GPCRs) and a proof-of-principle study for the 5HT_{1A}-receptor. The almost universal A¹⁰⁰ activation index, which depends on five inter-helix distances, is used as the single collective variable in well-tempered multiple-walker metadynamics simulations. Here we show free-energy profiles for the serotonin receptor as binary (apo-receptor + G-protein- α -subunit and receptor + ligand) and ternary complexes with two prototypical orthosteric ligands; the full agonist serotonin and the partial agonist aripiprazole. Our results are not only compatible with previously reported experimental and computational data, but they also allow differences between active and inactive conformations to be determined in unprecedented atomic detail, and with respect to the so-called microswitches that have been suggested as determinants of activation, giving insight into their role in the activation mechanism.

INTRODUCTION

Enhanced-sampling approaches such as metadynamics have become essential tools for exploring the configuration space of macromolecular biosystems, including G-protein coupled receptors (GPCRs). GPCRs are involved in many physiological processes and are the most frequent targets of approved drugs. Like most membrane proteins, GPCRs are characterized by high flexibility and often marginal stability. Each receptor contributes to the activation of specific cellular responses through versatile and complex downstream signaling that involves receptor activation and intracellular recruitment of either heterotrimeric G proteins or arrestins.

A mass of experimental evidence has been gathered in the past two decades that allows a consensus model for GPCR activation.³ However, despite the rapid progress towards understanding, the activation mechanism of these important receptors still needs to be characterized fully at atomic-level resolution.^{4,5} This would allow us not only to understand the biophysical basis of signaling, but also provide the knowledge necessary to design more effective and less toxic drugs.

Very recently, the first G-protein coupled structure of the serotonin receptor 5-HT_{1A} has been solved by cryo-EM.⁶ The 5-HT_{1A} receptor, a Class A GPCR, is a member of the serotonergic receptor family, which is found in the central and peripheral nervous systems and activated by the neurotransmitter serotonin (5-hydroxytryptamine, 5-HT). Although the 5-HT_{1A} receptor subtype is among the most studied, since it is an important therapeutic target for several neuropsychiatric disorders including anxiety, depression, and schizophrenia,⁷ the structural basis involving receptor dynamics, ligand efficacy and receptor activation is largely unknown.⁸

Force-field-based molecular dynamics (MD) simulations have already played a major role in revealing details of the activation process of GPCRs. 9,10,11,12,13 Moreover, MD simulations can provide insight into wild type receptors, which are often experimentally inaccessible. 14

Initially, very long simulations demonstrated the transition between active and inactive conformations.¹⁵ Later coarse grained but accurate force-field simulations allowed the complete characterization of the free-energy landscape for a GPCR mode of action, ^{16,17} but did not resolve individual receptor conformations in atomistic detail.

Specialized hardware,¹⁵ cloud-based computing resources,¹¹ or enhanced-sampling approaches are needed to capture the complex conformational changes that comprise the GPCR-activation process. Various enhanced-sampling algorithms¹⁸ have been used to sample the dynamics of GPCRs, including the string method,^{19,20} and methods based on collective variables (CVs) such as metadynamics.²¹

Our positive experience with GPCR binding/unbinding simulations 22 suggest that metadynamics is an effective technique for simulating such complex systems when a good set of CVs can be devised. To that end, one or more CVs must clearly distinguish the relevant states and enhance the sampling of the slow degrees of freedom involved in the process of interest. 23,24 Including all the slow variables is particularly difficult in complex systems such as GPCRs. This can be mitigated in part by combining metadynamics with replica-exchange algorithms, such as parallel tempering 25 or multiple walkers 26 that greatly improve the convergence of the free-energy reconstruction when using sub-optimal CVs. Our recent study of the activation mechanism for a class B GPCR involved extensive parallel tempering and multiple walker simulations where the chosen CVs were two combinations of the RMSD of the C α of the TM6 helix with the conformations of active and inactive receptor. 27 While the use of multiple replicas is able to overcome the limitations of the RMSD-based CVs, the associated computational cost is very high and structural knowledge of the active and inactive states is needed. A valid alternative is to use path-based CVs that capture the relevant degrees of freedom. 28 However, path-based CVs require not only the knowledge of active and inactive

states, but also an initial "guess" path connecting the two, which in the case of GPCRs is not trivial to obtain. Recently we proved it possible to define a generally applicable single CV for ligand binding/unbinding in class A GPCRs.²⁹ Here, we report a metadynamics-based multiple-walkers computational protocol that uses the general activation index A^{100} as a single activation CV. The A^{100} index³⁰ is defined as a linear combination of five distances between α -carbons of ten residues located on different helices and can thus be used within the PLUMED interface.^{31,32} Given the general applicability of the activation index A^{100} ^{30,33,34} the computational protocol introduced here can potentially be applied to all class A, rhodopsin-like GPCRs that exhibit the residues that occur in the A^{100} definition. As shown below, A^{100} , which was specifically designed to indicate the activation/deactivation state of the receptor, is better suited than microswitches such as the TM3-TM6 distance, which can be ambiguous with respect to activation.

The A¹⁰⁰ index was initially introduced as an analysis tool, and its use as a CV has been very recently reported to support experimental data rationalizing carvedilol's cellular signaling in the β₂-adrenergic receptor.³⁴ Here, we define the computational protocol exactly and describe its application to the serotonin 5-HT_{1A} receptor in its *apo*-form (ligand-free) and in the presence of two known ligands; the full agonist serotonin and the partial agonist aripiprazole. Apart from its simple definition and general applicability, further advantages of using A¹⁰⁰ with multiple walkers metadynamics are that no a priori knowledge of either the active or the inactive state is required, nor an initial path connecting the two states. The protocol still requires multiple walkers to converge the free-energy landscapes due to the fact that A¹⁰⁰ captures most but not all slow degrees of freedom, but compared to other CVs, such as the RMSD from crystallographic states, the number of walkers needed to converge the free energy is reduced. Moreover, we show that in the limit of converged free-energy surfaces, it is not only possible to gain insight into experimentally inaccessible intermediate states, but also to extrapolate

structural features of the receptor in the presence of ligands with different efficacies. This computational protocol satisfies a pressing need in GPCR research as it allows the systematical characterization of the activation/deactivation free-energy landscapes for class A GPCRs in unprecedented detail.

RESULTS AND DISCUSSION

Simulation time scales

The first task was to investigate the relaxation time of A^{100} in unconstrained simulations of the subject serotonin receptor (5-HT_{1A}). To monitor the deactivation of the receptor in the absence of a binding partner, similarly to previous simulations of the β_2 -adrenergic receptor, ¹⁵ we consider the equilibration of 5-HT_{1A} in its *apo*-active state, i.e., with no bound ligand, and binary complexes with serotonin and aripiprazole as representatives for full agonist and partial agonist ligands, respectively. We also include in the dataset complexes with the α -subunit of the G_i -protein trimer ($G_{\alpha i}$) to provide a reference for the stabilized active-like state of the receptor induced by the G-protein.³⁵ All the systems were equilibrated using single 2 μ s-long unconstrained simulations in the NPT ensemble; the last 0.5 μ s was used to determine the mean A^{100} -value.

The time-dependent A¹⁰⁰-plots for all 5-HT_{1A} systems are shown in 1. Starting point for the *apo*-5-HT_{1A} and 5-HT_{1A}-ligand binary complexes (Figures 1A, 1C and 1E) simulations were active cryo-EM structures⁶ (PDB accession codes 7E2X, 7E2Y, and 7E2XZ, respectively) from which the G-protein was removed. These three unconstrained simulations start at A¹⁰⁰-values of approximately 50 and give mean A¹⁰⁰-values of -17, -3, and -10 for the apo-5-HT_{1A}, 5-HT_{1A}-serotonin, and 5-HT_{1A}-aripiprazole respectively. These values are well within the inactive ranges defined for the two-state activation model.³⁰ The *apo*-receptor (Figure 1A) undergoes a

configurational change from its initial A^{100} -value of approximately 50 to values that oscillate around approximately -25 around 0.5 μ s. In our experience, this behavior is typical for simulations that start with the "wrong" conformation derived from modified experimental structures. It indicates that the *apo*-receptor prefers an inactive conformation that is accessible to unconstrained simulations within a few μ s. In contrast, the 5-HT_{1A}-serotonin simulation (Figure 1C) remains close to a A^{100} -value around zero throughout the 2 μ s simulation with excursions into the active (> 25) and inactive ranges. The 5-HT_{1A}-aripiprazole binary complex (Figure 1E) shows a steady decrease in A^{100} from a starting value around 50 to approximately -20 at 1.8 μ s, where it possibly stabilizes. Although this simulation is likely not converged, the above conclusions are consistent with the behavior found for 5-HT_{1A}-serotonin.

The rearrangement at approximately 0.5 μ s that leads to inactive A¹⁰⁰-values for the *apo*-receptor (Figure 1A) is accompanied by rearrangements in the highly conserved residues known as "microswitches" (Figures S1-4). These local structural changes identified previously and suggested to play an important role in receptor activation are:^{15,36} (a) the α -carbon distance between residues V^{6,34} and R^{3,50} as indicator of TM6 displacement, (b) the Y-Y motif as the c ζ distance between Y^{5,58} and Y^{7,53}, proposed as a stabilizing element of the active conformation, (c) root mean-square deviation (RMSD) to the active reference structure of the highly conserved residues N^{7,49}P^{7,50}xxY^{7,53} (NPxxY motif), which acts as an indicator of the reorientation of TM7, (d) the RMSD to the active structure of the PIF motif, involving residues P^{5,50}, I^{3,40}, and F^{6,44} that regulates receptor activation (details in Table S1).

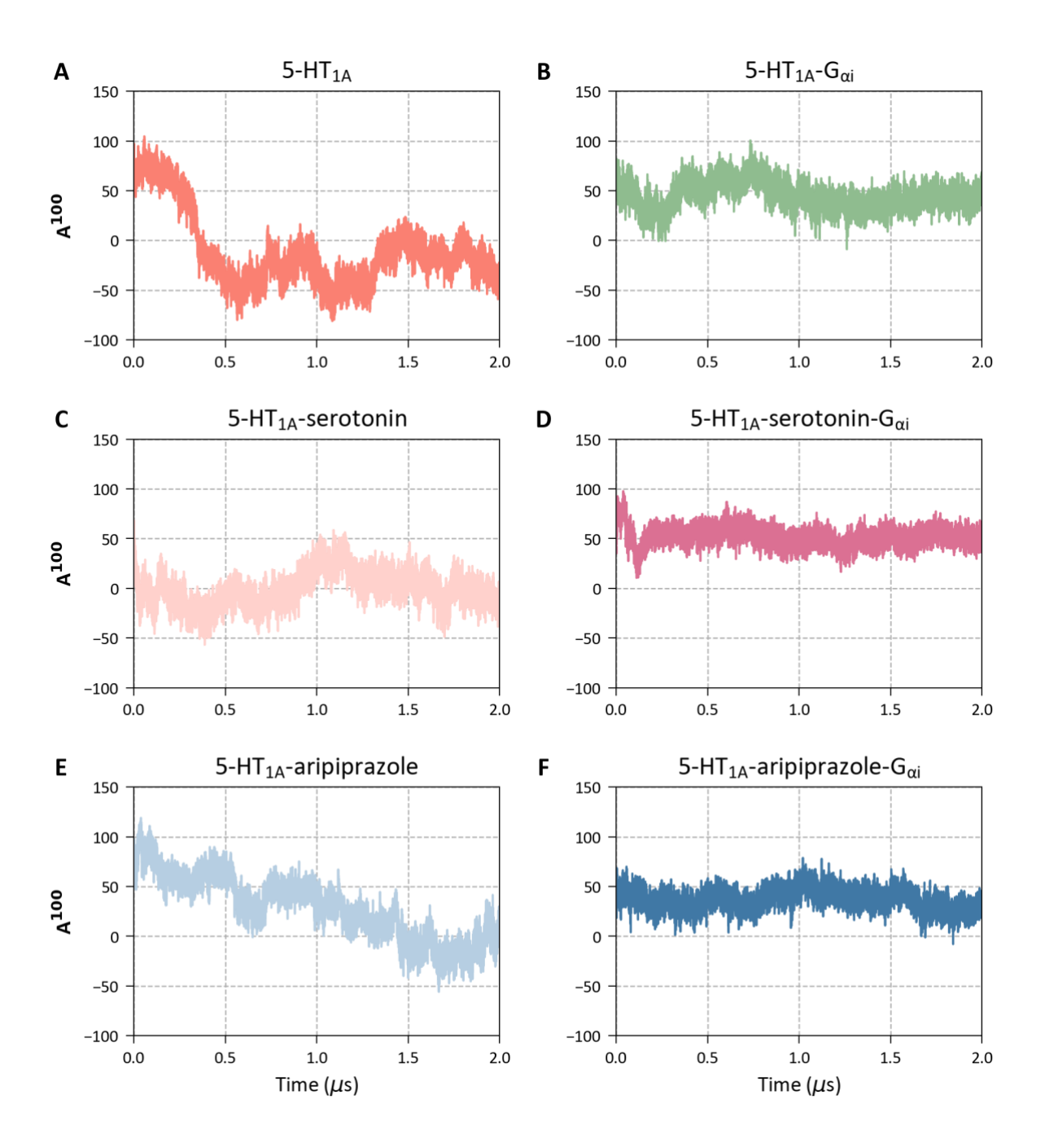


Figure 1. Time-dependence of A^{100} for all 5-HT_{1A} systems over 2 μs unconstrained molecular dynamics simulations.

For the *apo*-5-HT_{1A} receptor and 5-HT_{1A}-ligand binary complexes (Figures S1-4), the TM3-TM6 distance and YY motif occupy inactive-like conformations, while PIF and NPxxY motifs deviate from the starting active conformation, reaching values as high as 0.54 nm.

In contrast to the binary complexes, the ternary ligand- $5HT_{1A}$ - $G_{\alpha i}$ complexes (Figures 1B, 1D and 1F) show little change in A^{100} over the 2 μ s simulation time. Both stabilized active-like

conformations of the microswitches, and active mean A^{100} -values were obtained for all 5-HT_{1A} systems with bound G-protein. We therefore conclude that 2 μs unconstrained simulations are adequate to obtain equilibrated A^{100} -values.

Activity indices as cooperative variables

The A¹⁰⁰ index³⁰ was used as a single activation CV. Like RMSDs from a given structure, distance-based activity indices may be ambiguous in that drastically different receptor structures can be associated with the same A¹⁰⁰-value. This proves not to be a problem within the limited conformational space of the X-ray structures used for validation of A¹⁰⁰, as long as the walkers used for the production simulation and the metadynamics parameters are chosen carefully. Defining the optimal metadynamics parameters was the major task in developing the simulation protocol (see Methods for details).

Although A¹⁰⁰ has been used as a CV in a very recent publication,³⁴ its use is not straightforward, so that an exact simulation protocol was developed in order to obtain reliable activation/deactivation free-energy profiles. In end effect, the G-protein conformation must deviate very significantly from the activation pathway for structures to be generated that are not consistent with the original A¹⁰⁰ definition. This is not possible within the relatively short exploratory simulations used to generate the initial walker structures. Thus, the localized geometric nature of the structures that occur in the simulations reduces the ambiguity of A¹⁰⁰, so that it can be used as a CV. This is analogous to the widespread use of RMSDs as CVs. In our work on the glucagon receptor,²⁷ two-dimensional metadynamics simulations using two different RMSDs as CVs proved successful but only when combined with parallel-tempering or large scale multiple-walkers simulations. Moreover, the same set of RMSD-based CVs is not necessarily effective for class A activation (see steered MD simulation section in the

Supporting Information). This is an important practical consideration as the computational demand scales poorly with increasing numbers of CVs.

Implementing A¹⁰⁰ as a CV in PLUMED is straightforward as it involves only combining five distances linearly. However, selecting initial walkers for the multiple walker simulations and optimizing the metadynamics parameters can be challenging. To address this, unbiased MD simulations were used to obtain a distribution of structures across the CV range. From this distribution, walkers were chosen as starting points for the multiple walker simulations based on two criteria; an even distribution across the CV range and visual inspection to ensure they exhibited no obvious strong deviation from the expected structures (i.e. bad geometries of transmembrane domains, C- or N-terminus).

Once the walkers have been selected, optimal parameters for the multiple walker metadynamics simulations were determined with the goal of ensuring that walkers frequently and reversibly visit neighboring regions of the CV (i.e. those in which other walkers were initially placed) to reach convergence. CV fluctuations during the metadynamics run can be tracked by inspecting the individual trajectories for each walker (Figure 2C). Convergence can be assessed by monitoring i) the free-energy profiles as a function of time and ii) the Gaussian hills deposition over time, as shown in Figure 2A and 2B, respectively for the *apo-5HT*_{1A}-receptor. To avoid sampling unphysical conformational states of the receptor, hills were deposited every 1 ps with an initial height of 1.0 kJ/mol and a bias factor of 5. Thus, we favor a protocol in which the system is nicely and smoothly driven along the CV pathway.

11

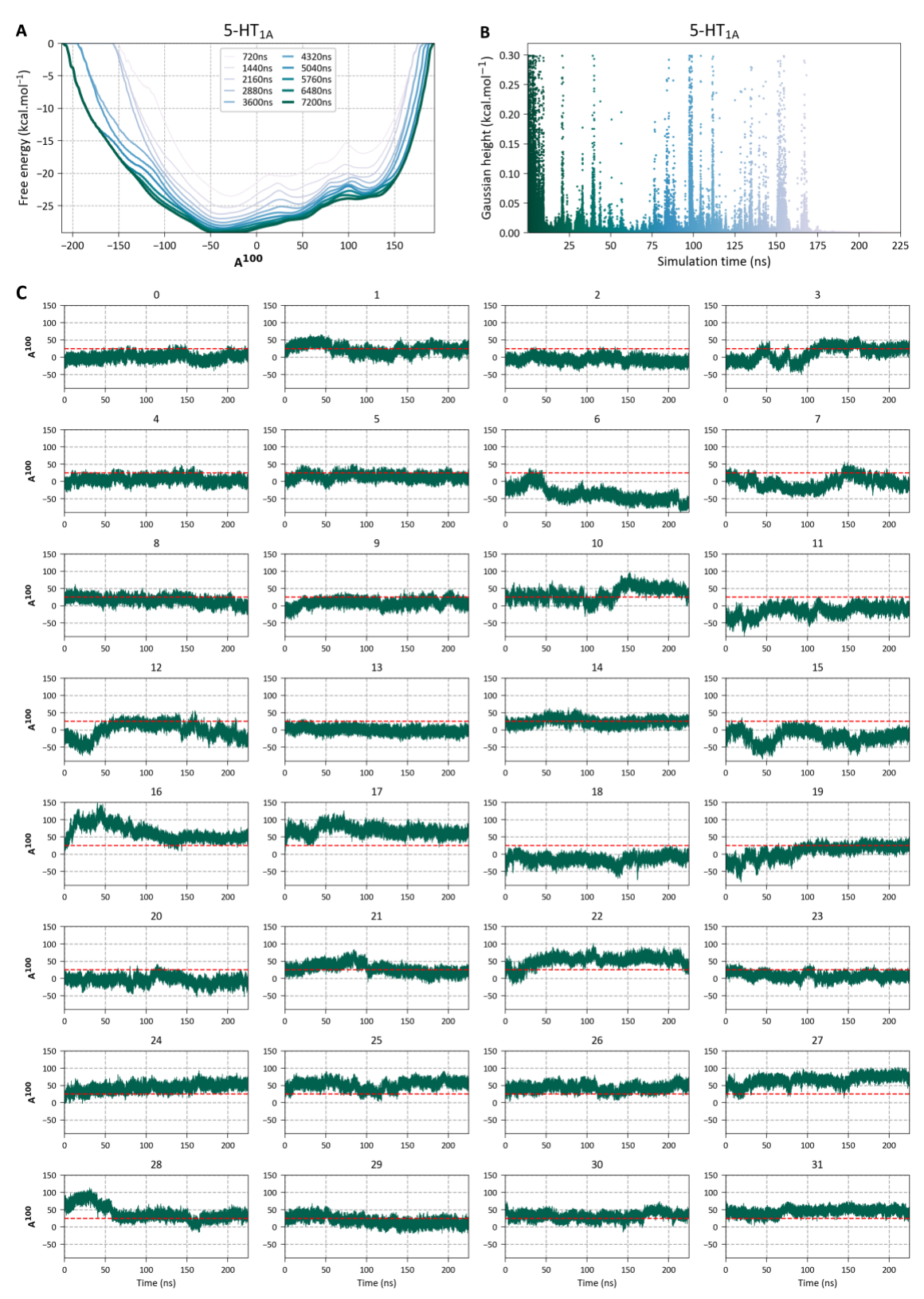


Figure 2. (A) Time-dependence of the calculated free-energy vs. A^{100} profile for the *apo-5-HT*_{1A} receptor. (B) Time evolution of the Gaussian hill height over simulation time. (C) A^{100} as a function of the simulation time for 32 walkers of the *apo-5-HT*_{1A} receptor. All these plots are used to determine the convergence of the multiple walker metadynamics simulations.

A further important check of the results is whether the minimum-energy conformations obtained from the free-energy profiles calculated with the metadynamics protocol are compatible with those obtained in unconstrained simulations on the same structures. Figure S10 shows the correlation between the mean A^{100} -value over the last 500 ns of 2 μ s unconstrained simulations and the deepest minimum found in the metadynamics simulations. The RMSD between the two is only 11.6 (mean unsigned error 7.2) and R^2 for the linear regression 0.91.

Activation/deactivation free-energy profiles

Free-energy profiles obtained for all 5-HT_{1A} systems are shown in Figure 3. The time evolution of the estimated free energy (Figure S11) and the Gaussian height (Figure S12) were used as convergence criteria for the metadynamics simulations. Figure 3A shows the activation/deactivation free-energy profiles of both *apo*-5-HT_{1A} and *apo*-5-HT_{1A}-G_{0i}. The *apo*-5-HT_{1A}-G_{0i} shows a deep minimum at $A^{100} = 44$, indicating a relatively inflexible active conformation. While the *apo*-5-HT_{1A} shows a minimum clearly in the inactive region, at $A^{100} = -43$, that spreads up to $A^{100} = -10$ with little increase in energy. This behavior may indicate a flexible inactive conformation that is not as well defined as the active minimum found with bound G_{0i} . Note, however, that A^{100} only considers the activation state of the receptor. Thus, the flat region of the free-energy profile between $A^{100} = -43$ and -10 does not necessarily indicate a single minimum. The distinction between a single flexible minimum and energetically very similar minima with activities in the range observed cannot be made from the current simulations. A shoulder that may indicate a metastable conformation is found at $A^{100} = 40$ ($\Delta\Delta$ G= 2.0 kcal mol⁻¹) and a metastable minimum at $A^{100} \approx 100$ ($\Delta\Delta$ G= 5.2 kcal mol⁻¹). These results are consistent with the high basal activity observed for the receptor.

The simulations with the endogenous ligand serotonin (Figure 3B) allow us to reconstruct a free-energy profile showing a minimum for the binary 5-HT_{1A}-ligand complex at $A^{100} = 7$, and a clear metastable shoulder in the active region at $A^{100} \approx 39$ -63 ($\Delta\Delta G = 0.8$ kcal mol⁻¹). The 5-HT_{1A}-serotonin- $G_{\alpha i}$ ternary complex shows a narrow minimum at $A^{100} = 51$ and a very unstable shoulder at $A^{100} = -20$ ($\Delta\Delta G = 9.8$ kcal mol⁻¹).

Figure 3C shows the free-energy profile obtained for 5-HT_{1A} complexes with the partial agonist aripiprazole. A minimum and a shoulder 0.4 kcal mol⁻¹ higher in energy (A^{100} = -15 and A^{100} \approx 6-10, respectively) are found for the 5-HT_{1A}-aripiprazole binary complex in the inactive region. Two additional shoulders can be observed in the active region at A^{100} \approx 26-32 ($\Delta\Delta G$ = 0.8 kcal mol⁻¹) and A^{100} \approx 58-65 ($\Delta\Delta G$ = 2.1 kcal mol⁻¹). In contrast to the results for the binary complex, a single minimum at A^{100} = 31 is observed for the 5-HT_{1A}-aripiprazole- $G_{\alpha i}$ ternary complex.

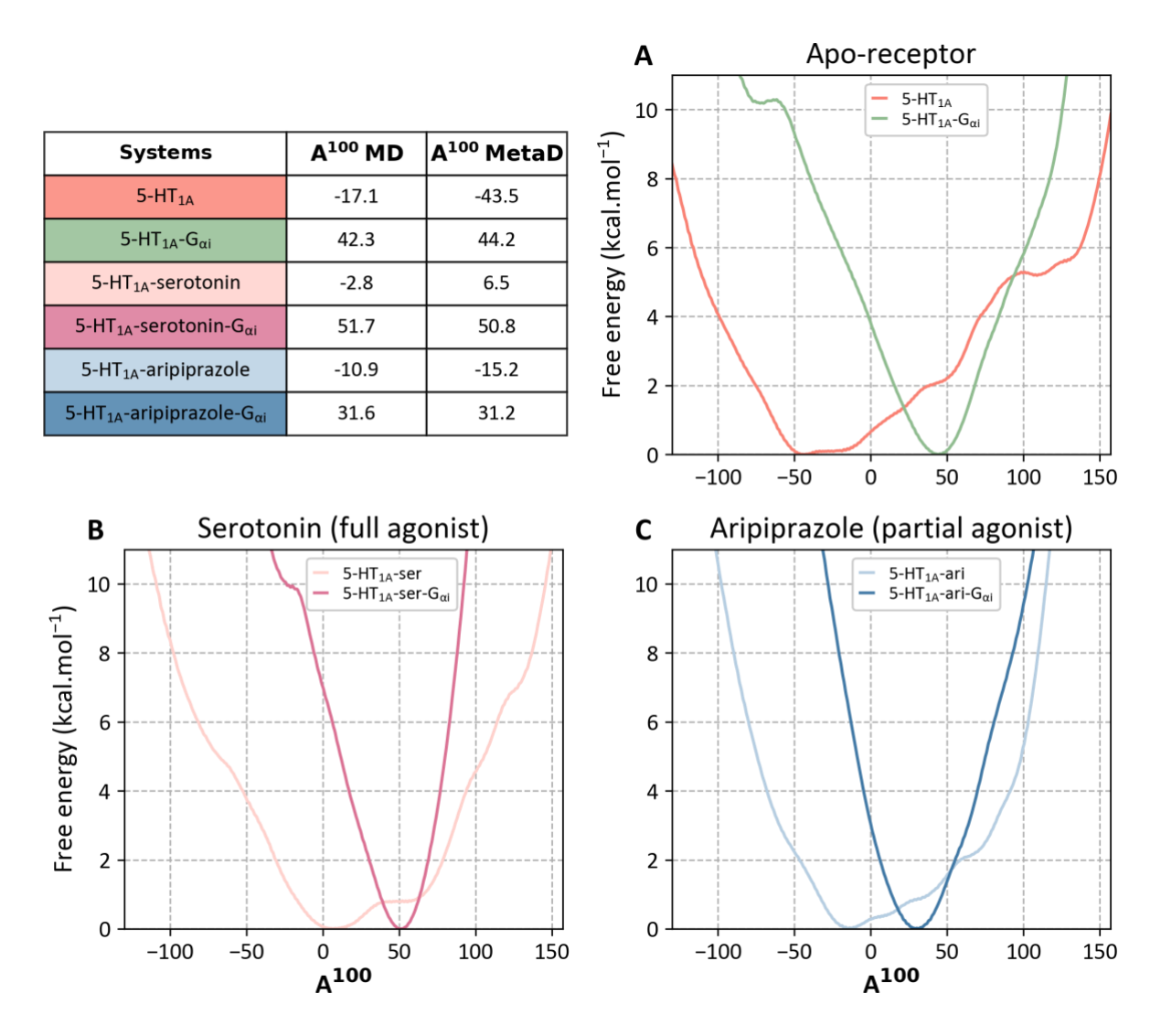


Figure 3. Simulation results for 5-HT_{1A} systems. Calculated activation/deactivation free-energy profiles from metadynamics simulations. The mean A^{100} -values for the last 500 ns of the unbiased simulations and the A^{100} values corresponding to the lowest minima in the free-energy curves are also reported.

Note that the position of the A^{100} -minimum does not necessarily correlate with absolute activity,³⁰ which is also affected by factors other than the receptor conformation alone. In particular, A^{100} -minima for *apo*-complexes likely relate to the ability of the *apo*-receptor to recruit the G-protein, which is not necessarily the same as the level of activity.

Modulation of 5-HT_{1A} dynamics by ligands

Because the A¹⁰⁰ index is a linear combination of inter-residue distances, it does not map uniquely to individual structures. It was also not designed to differentiate between intermediate

and fully active conformations. The active A^{100} -range (≥ 25 in the two-state model) encompasses TM3-TM6 distances (Figure S5) in the range assigned to the inactive and intermediate conformations, ¹⁵ approximately 0.8-1.9 nm. The same is true of the YY distance (Figure S6), NPxxY (Figure S7), and PIF motifs (Figure S8). These observations confirm that A^{100} is less ambiguous as an activation CV than either the TM3-TM6 distance, YY distance, the NPxxY or PIF motifs. Therefore, to obtain a detailed analysis of how conformational changes induced by ligands binding propagate through the receptor, the roles of conserved microswitches were assessed by comparing free-energy landscapes in the absence and presence of bound agonists. For this purpose, our A^{100} metadynamics simulations were reweighted to reconstruct 1D and 2D free-energy landscapes with respect to the microswitches.

Figure 4 shows 1D free-energy landscapes projected onto the relevant microswitches. The *apo*-5-HT_{1A} system clearly shows minima compatible with inactive-like conformations (0.98 nm, 1.45 nm, 0.40 nm, 0.49 nm for the TM3-TM6 distance, YY distance, NPxxY and PIF motif, respectively), whereas less inactive- or even intermediate-like conformations can be adopted by 5-HT_{1A}-ligand systems. Both serotonin and aripiprazole binary complexes exhibit intermediate-like conformations for the NPxxY motif (0.25 nm). The 5-HT_{1A}-serotonin system shows an intermediate-like conformation for the YY distance (0.99 nm) and the PIF motif (0.29 nm), and inactive-like conformation for the TM3-TM6 distance (0.94 nm). Conversely the 5-HT_{1A}-aripiprazole binary complex shows inactive-like conformations for the YY distance (1.45 nm) and PIF motif (0.37), and an intermediate-like conformation for the TM3-TM6 distance (1.17 nm).

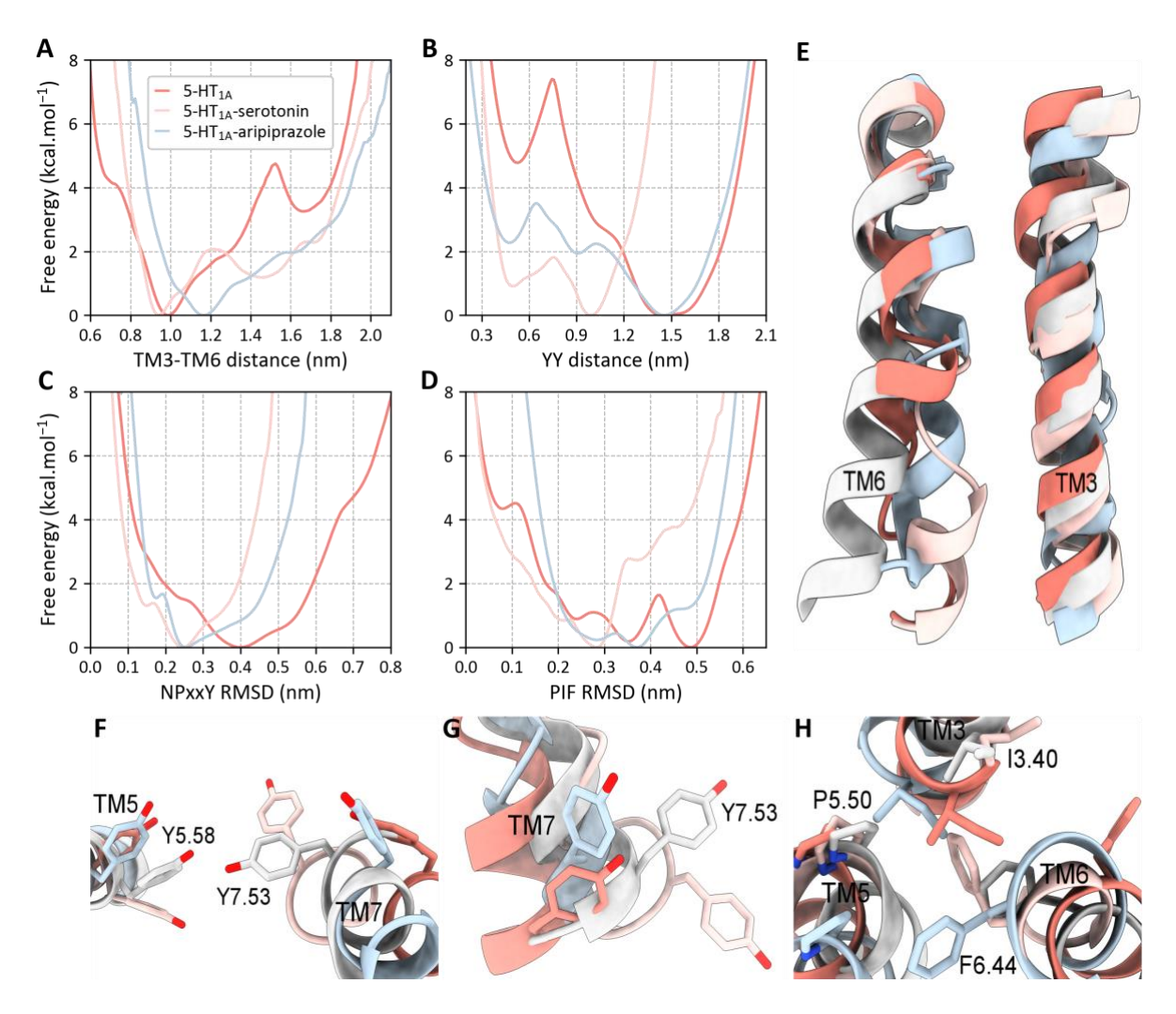


Figure 4. Comparison of 5-HT_{1A} inactive systems. (A-D) 1D free-energy landscapes projected as a function of the microswitches. Representation of microswitches: (E) TM3-TM6 distance, (F) YY motif, (G) NPxxY motif, (H) PIF motif. *Apo*-5HT_{1A}, 5-HT_{1A}-serotonin and 5-HT_{1A}-aripiprazole systems are shown in salmon, light pink, and light blue respectively. Active cryo-EM structure 7E2Y is represented in white.

Because it is well established that outward movement of TM6 upon ligand binding is one of the most prominent features of GPCR activation,^{38,39} we also projected the results of the A¹⁰⁰ metadynamics simulations onto free-energy landscapes relative to a combination of the TM3-TM6 distance with the other microswitches considered here. The resulting 2D free-energy landscapes are shown in Figure 5. Several clear minima spanning regions compatible with active-, intermediate- and inactive-like states are found in the free-energy profiles. In the absence of a bound agonist, the receptor adopts both active and inactive conformations of TM6,

with the minimum of the free energy located at inactive states of the TM3-TM6 distance, YY, NPxxY, and PIF motifs. (Figures 5A, D, and G, respectively).

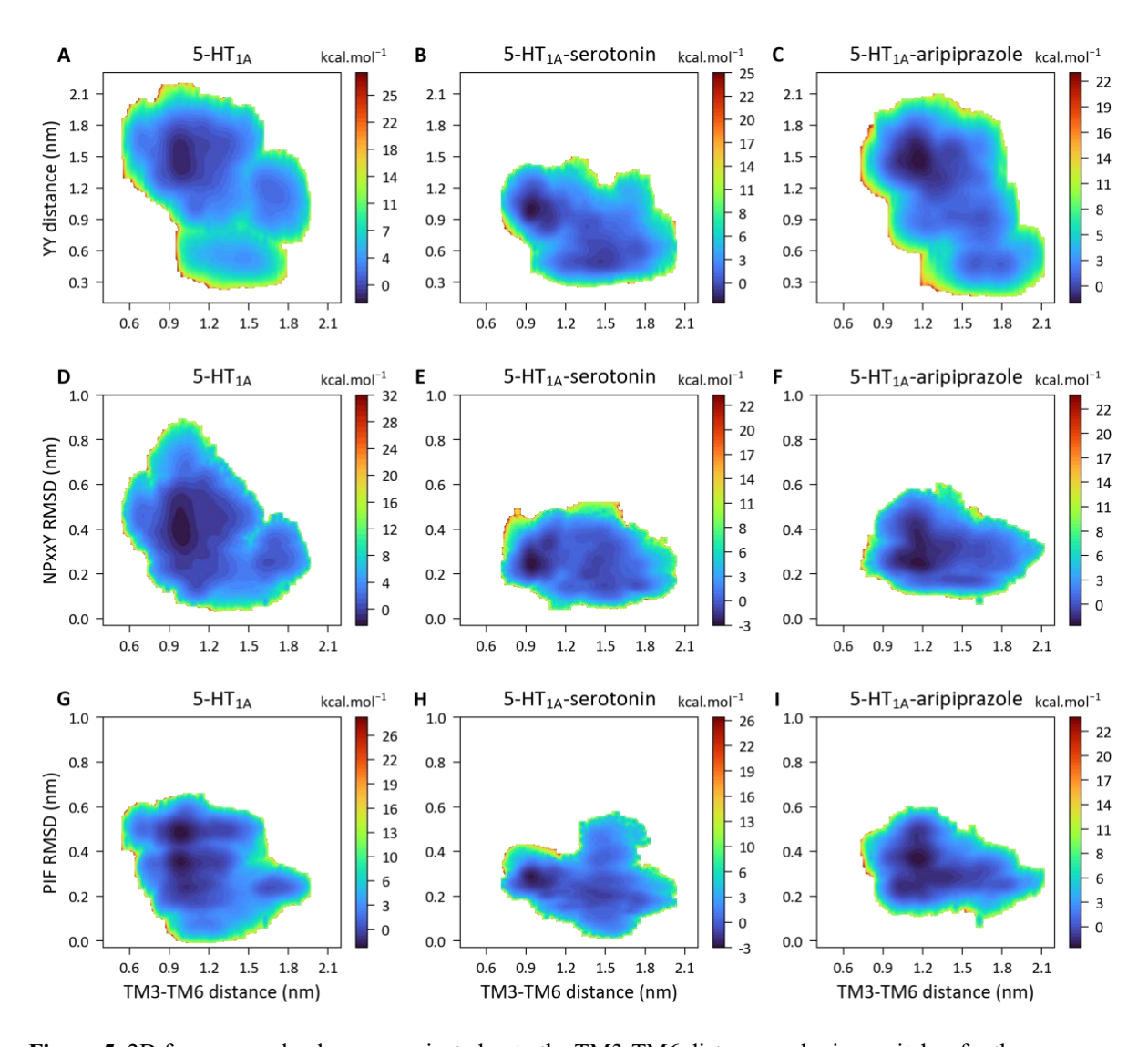


Figure 5. 2D free-energy landscapes projected onto the TM3-TM6 distance and microswitches for the *apo* receptor and all 5-HT_{1A} binary systems.

In the presence of the full agonist serotonin, both inactive and active conformations of TM6 are populated and the YY motif can assume an almost active-like (or intermediate) state, even when TM6 adopts an inactive-like conformation (Figure 5B). In contrast, a remarkably large range of the YY distances is induced by the partial agonist aripiprazole (Figure 5C). For both ligands, active- and inactive-like states of the TM3-TM6 distance are accessible when the conformation of the NPxxY motif mostly populates an intermediate-like state. On the other

hand, the minimum of the PIF motif is shifted toward a less inactive-like state (or intermediate state) in the case of the full agonist serotonin in comparison to aripiprazole (Figures 5H and I, respectively). These results are not only consistent with the notion that ligands can stabilize different receptor states⁴⁰ but also suggest that binding of a full agonist reduces the number of inactive-like states of the conserved microswitches in comparison to a partial agonist.

Since the chemical nature of the ligand must be the cause of the structural variation observed in the microswitches, specific interactions between the ligand and the receptor were assessed through hydrogen-bond analysis. Figures 6C and 6D show the hydrogen-bond occupancy of 5-HT_{1A}-ligand systems. For both 5-HT_{1A}-serotonin and 5-HT_{1A}-aripiprazole binary complexes, hydrogen-bond interactions are formed with the conserved residues D^{3,32} and N^{7,39}, which play a vital role in the stabilization of aminergic ligands in the binding pocket. Besides these common interactions in TM3 and TM7, a different occupancy pattern can be observed between ligands. While serotonin stabilizes conformational changes in TM5, TM6, and TM7 prior to G-protein coupling, hydrogen-bond interactions between aripiprazole and the receptor are concentrated on extracellular residues in TM7.

Consistent with prior experimental studies,⁴³ a specific hydrogen-bond interaction between the serotonin hydroxyl group and the S^{5,42} sidechain can be observed from Figures 6A and 6C. In contrast, aripiprazole lacks the hydroxyl group, and has chlorine atoms on the phenyl ring, so that a specific polar interaction with residues in TM5 cannot be formed (Figures 6B and 6D). Mutagenesis and computational studies have shown serine residues in TM5 to be important for activation of the adrenergic and serotonergic receptors.^{43,44,45}. Besides, it has been suggested that TM5 is more closely connected with ligand specificity than the other transmembrane segments.⁴⁶ Thus, while the conserved D^{3,32} in TM3 is important for coordinating the amino functionality, the least well conserved TM5 has been pointed out to be the most important

transmembrane domain for interactions with a significant but variable part of the ligand molecule. Therefore, ligands can exercise direct control over TM5 through distinct interaction patterns, generating a variety of ligand-specific conformational states.

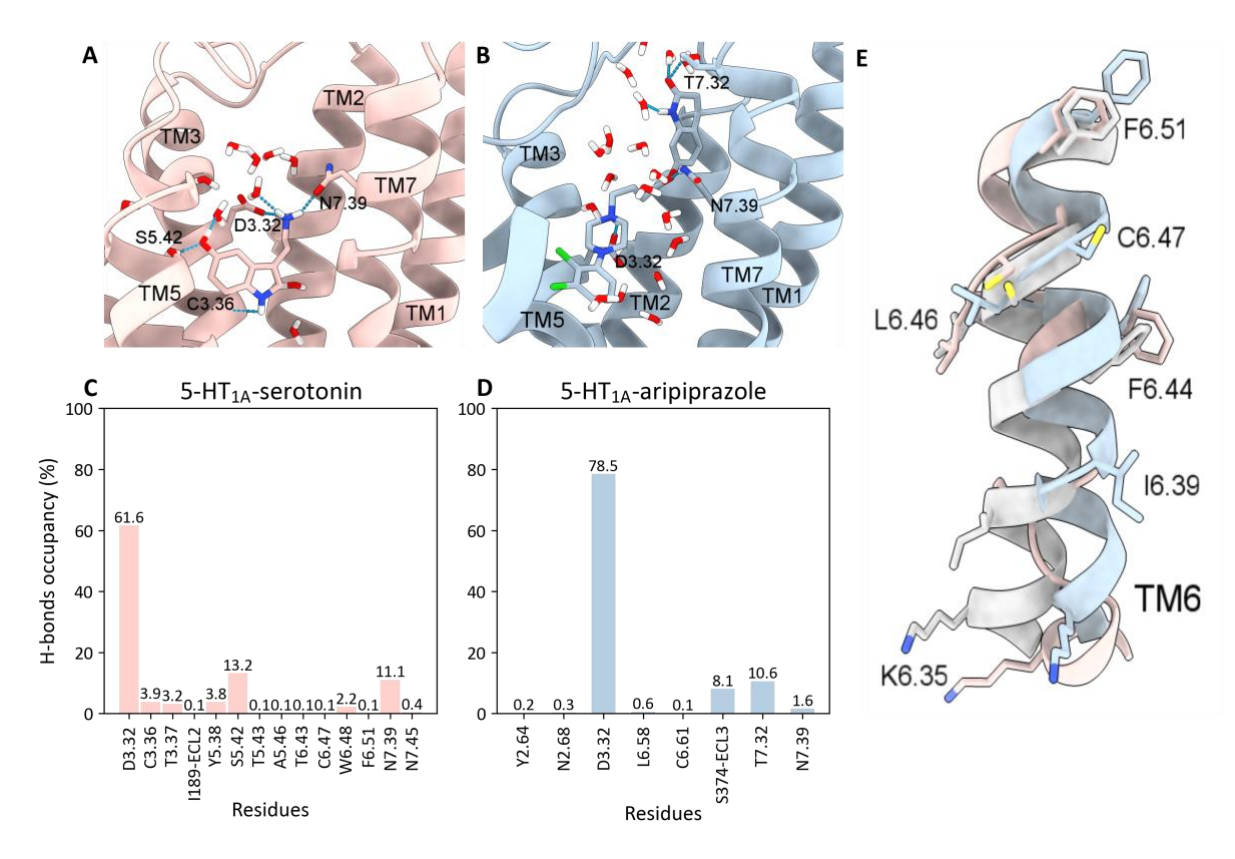


Figure 6. Comparison of 5HT_{1A}-ligand binary complexes. (A-B) Representation of polar interaction network formed in the binding pocket. (C-D) Hydrogen-bond occupancy. (E) Representative view of the TM6 conformational rearrangement. 5-HT_{1A}-serotonin and 5-HT_{1A}-aripiprazole binary complexes are shown in light pink and light blue respectively. Active cryo-EM structure 7E2Y is shown in white.

It has been proposed that the activation of aminergic receptors occurs sequentially. ⁴⁷ Once the primary contacts with TM3 and TM5 are established, ligands induce structural changes in TM6 that facilitate the binding and activation of a G-protein at the intracellular site of the receptor. TM6 conformational changes, first bending and then rotation, have been associated with rearrangements of the PIF motif. ^{48,49,50,51} This likely explains structural differences between 5-HT_{1A}-ligand binary complexes in the PIF motif and TM6. While the full agonist serotonin stabilizes an intermediate-like state of the PIF motif (Figures 4D and 4H), the inactive-like

state adopted by 5-HT_{1A}-aripiprazole binary complex might be associated with the observed TM6 counterclockwise rotation relative to the active 5-HT_{1A}-serotonine-G_i cryo-EM structure (Figure 6E). These subtle but distinct local structural differences that lead to non-optimal G-protein activation have been related to partial agonism at different sub-families of GPCRs. ^{4,50,51}

Although hydrogen-bond interactions between agonists and TM5 have not been reported in cryo-EM structures of 5-HT_{1A}-ligand-G_i complexes, a mechanistic rationale might explain these discrepancies. According to structural and experimental data, the intracellular and extracellular ends of TM6 move in opposite directions upon G-protein binding, corresponding to a pivoting motion of TM6 around its center close to the conserved residue P^{6.50} ⁵² Thus, the intracellular end moves outward while the extracellular one moves towards the orthosteric binding pocket, which results in the compression of the ligand binding pocket in the fully active conformation.³⁸

The ligand-binding pocket is compared for all 5-HT_{1A}-ligand systems in Figure S13. As a consequence of receptor deactivation, the extracellular half of TM6 is positioned away from the binding pocket, as indicated by the displacement of residue $A^{6.55}$ in Figure S14, which leads to a larger binding pocket. The structural differences in the orthosteric ligand-binding pocket between aripiprazole binary and ternary complexes are relatively subtle. However, in the absence of the G-protein, the smaller and more flexible full agonist serotonin can insert itself more deeply into the binding pocket with its hydroxyl group forming polar interactions with residues in TM5. Even though the binding pocket in 5-HT_{1A}-serotonin- G_{0i} is sterically hindered by TM6 motion, a hydrogen-bond interaction between the nitrogen of the indole moiety in serotonin and the backbone carbonyl of $S^{5.42}$ can still be formed (Figure S15). Therefore, structural comparisons between binary and ternary complexes demonstrate that an attenuated polar interaction network in ternary complexes might be attributed to conformational changes

in the orthosteric binding pocket upon G-protein binding (Figure S13). This strong differentiation suggests a potential role of the polar interaction network as a regulator in the initial stages of the signal transduction mechanism in receptor activation.

The binding pocket of the receptor in the absence of bound ligands was also investigated. Figure 7 clearly reveals water molecules forming hydrogen bonds interactions with residues S^{5,42}, D^{3,32}, N^{7,35} and a sodium ion that mimics the electrostatic interaction between the positively charged amine of aminergic ligands and residue D^{3,32}. Thus, for both *apo*-receptor systems the presence of water molecules and Na⁺ resembles the three polar functionalities found in the 5-HT_{1A}-serotonine binary complex. Notably, a more extensive rod of water molecules in proximity with residue S^{5,42} can be found for the *apo*-5HT_{1A}-G_{αi} (Figure 7D), in comparison to *apo*-5-HT_{1A}. This water-molecule network contributes to the stabilization of 5-HT_{1A} in the active conformation.⁶

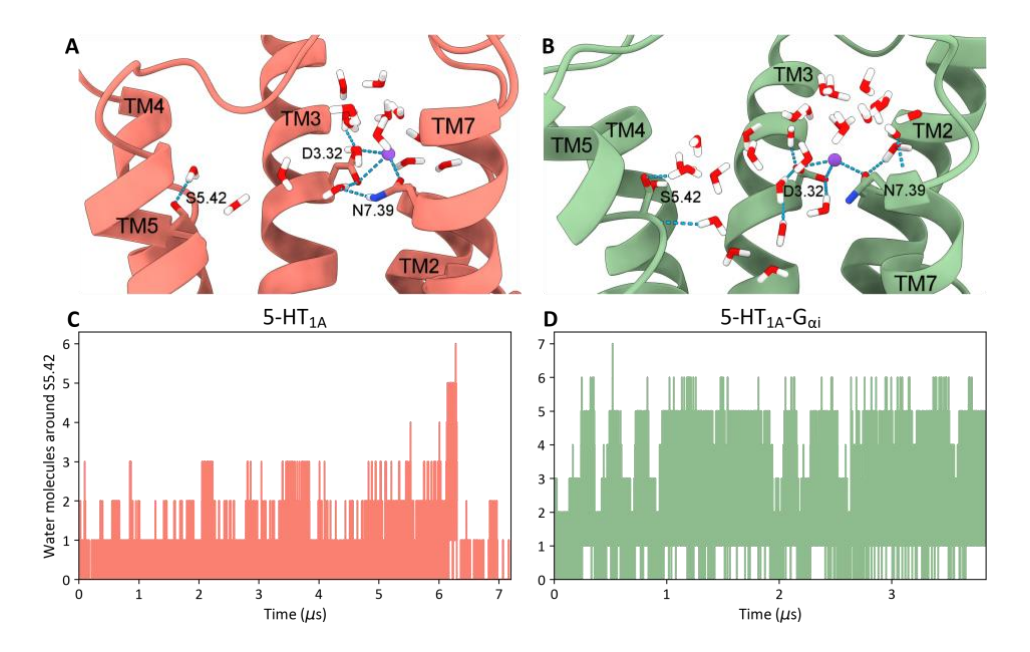


Figure 7. Comparison of *apo*-5HT_{1A} systems. (A-B) Representation of polar interactions within the binding pocket of *apo*-5HT_{1A} systems. Water molecules around residues $S^{5.42}$, $D^{3.32}$ and $N^{7.39}$ with a cut-off distance lower than 5 Å are displayed (C-D) Number of water molecules around residue $S^{5.42}$ were calculated with a cut-off distance of 3 Å. *Apo* receptors 5-HT_{1A} and 5-HT_{1A}-G_{αi} are shown in salmon and green respectively.

CONCLUSIONS

The simulation protocol described here allows us to determine free-energy profiles for the activation/deactivation process of the serotonin 5-HT_{1A} receptor, and we are confident that this protocol can be used to characterize the activation for all Class A GPCRs for which the A¹⁰⁰-activity index can be determined. ³⁰ Note that A¹⁰⁰ was trained using data from the muscarinic M_2 , histamine H_4 (human and mouse wild types and mutants), β_2 -adrenergic and μ -opioid receptors and was validated using experimental data from a total of 54 receptors. In a separate study, we have used the protocol for an extensive study of the β_2 -adrenergic receptor with similar success to that reported here for 5-HT_{1A} and very recently a paper was published reporting A¹⁰⁰ free-energy profiles to support experimental data. ³⁴ Given that A¹⁰⁰ is rapidly gaining acceptance as a general activation measure, ³³ and considering the reliability of the optimized protocol described here, we are confident to have described a metadynamics simulation technique that is superior to other activation CVs, for instance the TM3-TM6 distance, because these may be ambiguous for some receptor situations, as described above.

The results described here for the 5-HT_{1A} receptor are fully compatible with the known experimental results and reproduce the experimentally deduced mechanistic features. Thus, the simulations allow us to reach several important conclusions about the activation mechanism of 5-HT_{1A} .

The computed free-energy landscapes, specific interaction analysis and structural inspection suggest a combined mechanism that requires the action of both stabilizing intracellular and extracellular interactions in the receptor core for the full activation of the receptor. We have demonstrated the potential role of polar interaction networks in the receptor core as a regulator in the initial stages involved in receptor activation. In addition, we have provided details of the molecular basis for the basal activity of the receptor and have obtained detailed structural

insights that rationalize the mechanism of action of ligands with different efficacies at the 5-HT_{1A} receptor.

The free-energy profiles obtained from the simulations are simpler than might have been expected, but the simulations are consistent with a conformational-selection, rather than an induced-fit mechanism.⁴ In summary, we have described a computational protocol that we expect to be quite general for activation/deactivation free-energy profiles of Class A GPCRs. It allows both the number and the relative stabilities of the competing conformations to be determined. Thus, the present proof-of-principle simulations provide impressive support for the conformational selection mechanism of receptor activation for 5-HT_{1A}.

COMPUTATIONAL METHODS

Systems preparation

The structural models for this study were based on cryo-EM structures of the 5-HT_{1A} receptor bound to different ligands and the G_i-protein.⁶ (Details in the Supporting Information).

General setup of the MD simulations

All unbiased MD simulations were performed using GROMACS 2019.4.⁵³ Periodic boundary conditions were applied in all directions. The simulations were run at constant pressure and temperature in the NPT ensemble. The Berendsen barostat⁵⁴ was applied to maintain a pressure of 1 bar. The temperature was held constant at 310 K with temperature coupling being achieved by the V-rescale thermostat⁵⁴ in three separate coupling groups for (i) solvent and ions, (ii) protein and ligand, and (iii) the DOPC membrane. Bonds involving hydrogen atoms were constrained using the LINCS algorithm,⁵⁵ enabling a time step of 2 fs. A cutoff of 12 Å was used for short-range van der Waals interactions. Particle mesh Ewald (PME)⁵⁶ was used to treat electrostatic interactions, using a cutoff distance of 12 Å. All simulations used the SPC/E water

model.⁵⁷ 5-HT_{1A}- $G_{\alpha i}$ systems included a box size of 9.5×9.6×19.9 nm³ with 38,000 water molecules, and 278 DOPC molecules, whereas 5-HT_{1A} systems without $G_{\alpha i}$ compromised a box of 9.5×9.6×13.0 nm³ with 25,000 water molecules and 278 DOPC molecules.

Metadynamics simulations

Metadynamics simulations in the well-tempered variant (WT)⁵⁸ were performed to estimate the activation free-energy profiles. The simulations were run in the multiple walkers²⁶ scheme using 32 walkers at 310 K. Our A¹⁰⁰ activation index³⁰ (equation (1)) was used as the single collective variable for the applied metadynamics history-dependent bias.

$$A^{100} = 14.43R^{V^{1.53}-R^{7.55}} - 7.62R^{D^{2.50}-T^{3.37}} + 9.11R^{T^{3.42}-A^{4.42}} - 6.32R^{K^{5.66}-L^{6.34}} - 5.22R^{H^{6.58}-Y^{7.35}} + 278.88$$
(1)

where the distances R are measured between the α -carbon atoms of the residues given in the superscript.

Representative structures for each model were extracted from the 2μs unconstrained molecular dynamics trajectory along the reaction coordinate, spanning a range between active and inactive conformations. Based on these structures, the multiple walker technique²⁶ was conducted in the well-tempered variant.⁵⁸ Gaussian hills with initial height of 0.24 kcal mol⁻¹ were applied every 1 ps with a bias factor of 5, and the Gaussian width was set to 0.1 nm. Free energies were calculated using the sum hills function of the PLUMED 2.5.3 plug-in.^{31,32} Convergence was assessed by monitoring the time evolution of the estimated free energy and the evolution of the Gaussian height during the A¹⁰⁰ metadynamics simulations. Depending on the system, a full free-energy profile converges in 3040-7200 ns collective simulation time. Free-energy profiles as a function of the microswitches were computed by reweighting of the A¹⁰⁰ metadynamics simulations according to the algorithm described in ref 59. The calculation

of the reweighting factor c(t) was enabled by using the keyword CALC_RCT during the metadynamics simulations and metadynamics trajectories were post-processed with the driver function of PLUMED.

Hydrogen-bond interactions with a default cutoff distance and angle of 3 Å and 135°, respectively, were performed with CPPTRAJ module of AmberTools18.⁶⁰ Water molecules with a cutoff distance 3 Å were estimated with the gmx trjorder functionality of Gromacs. UCSF Chimera⁶¹ was used for data analysis and visualization, and plots were created with Matplotlib.⁶²

ASSOCIATED CONTENT

Supporting Information. 5-HT_{1A} systems preparation protocol; microswitches definition; time-series plots for: i) A¹⁰⁰, ii) TM3-TM6 distance, iii) YY distance, iv) NPxxY RMSD, v) PIF RMSD; dispersion plots showing A¹⁰⁰ as a function of: i) TM3-TM6 distance, ii) YY distance, iii) NPxxY RMSD, iv) PIF RMSD; steered MD simulation protocol and results; correlation plot between the mean A¹⁰⁰-value from MD runs and the deepest minimum identified in the A¹⁰⁰ free-energy profiles; A¹⁰⁰ free-energy profiles reconstructed at increasing metadynamics sampling times; time evolution of the Gaussian hill height during the metadynamics simulations; comparison of the orthosteric pocket in 5-HT_{1A} binary and ternary complexes; representation of A^{6.55} outward displacement; comparison of 5-HT^{1A} ternary complexes in terms of: i) polar interaction network in the binding pocket and ii) hydrogen bond occupancy (PDF)

Data Availability Statement

All input data for the simulations ran and analyzed during this study have been deposited to the public repository of the PLUMED consortium, PLUMED-NEST (plumID:23.005).

26

AUTHOR INFORMATION

Corresponding Authors

*Timothy Clark, Tim.Clark@fau.de * Francesco Luigi Gervasio,

Francesco.Gervasio@unige.ch.

Author Contributions

The manuscript was written through contributions of all authors. All authors have given

approval to the final version of the manuscript.

Funding Sources

Work in Erlangen was supported by the Deutsche Forschungsgemeinschaft as part of Research

Training Group GRK 1910 "Medicinal Chemistry of Selective GPCR Ligands" and by grants

of supercomputer time from the Gauss Alliance on SuperMUC (Project Nr. Pr74su) and from

the Erlangen National High Performance Computing Center (NHR@FAU) of the Friedrich-

Alexander-Universitaet Erlangen-Nuernberg (FAU). NHR funding was provided by federal

and Bavarian state authorities. NHR@FAU hardware was partially funded by the DFG-Grant

No. 440719683.

We acknowledge PRACE and the Swiss National Supercomputing Centre (CSCS) for large

supercomputer time allocations on Piz Daint, project IDs: pr126, s1107. FLG acknowledges

the Swiss National Science Foundation and Bridge for financial support (projects number:

200021 204795 and 40B2-0 203628).

ABBREVIATIONS

5-HT_{1A}, serotonergic receptor; MD, molecular dynamics; PDB, Protein Data Bank; RMSD, root mean squared deviation; TM, transmembrane; 1D, one-dimensional; 2D, two-dimensional; CV, collective variable.

REFERENCES

1 Bjarnadóttir, T. K.; Gloriam, D. E.; Hellstrand, S. H.; Kristiansson, H.; Fredriksson, F.; Schiöth, H. B. Comprehensive Repertoire and Phylogenetic Analysis of the G protein-Coupled Receptors in Human and Mouse. *Genomics* **2006**, *88*, 263–273.

2 Hauser, A. S.; Attwood, M. M.; Rask-Andersen, M.; Schiöth, H. B.; Gloriam, D. E. Trends in GPCR Drug Discovery: New Agents, Targets and Indications. *Nat. Rev. Drug. Discov.* **2017**, *16*, 829–842.

3 De Lean, A.; Stadel, J. M.; Lefkowitz, R. J. A Ternary Complex Model Explains the Agonist-Specific Binding Properties of the Adenylate Cyclase-Coupled Beta-Adrenergic Receptor. *J. Biol. Chem.* **1980**, *255*, 7108–7177.

4 Deupi, X.; Kobilka, B. K. Energy Landscapes as a Tool to Integrate GPCR Structure, Dynamics, and Function. *Physiology (Bethesda)* **2010**, *25*, 293–303.

5 Weis, W. I.; Kobilka, B. K. The Molecular Basis of G Protein-Coupled Receptor Activation. *Ann. Rev. Biochem.* **2018**, *87*, 897–919.

6 Xu, P.; Huang, S.; Zhang, H.; Mao, C.; Zhou, X. E.; Cheng, X.; Simon, I. A.; Shen, D. D.; Yen, H. Y.; Robinson, C. V.; Harpsoe, K.; Svensson, B.; Guo, J.; Jiang, H.; Gloriam, D. E.; Melcher, K.; Jiang, Y.; Zhang, Y.; Xu, H. E. Structural Insights into the Lipid and Ligand Regulation of Serotonin Receptors. *Nature* **2021**, *592*, 469–473.

7 Barnes, N. M.; Ahern, G. P.; Becamel, C.; Bockaert, J.; Camilleri, M.; Chaumont-Dubel, S.; Claeysen, S.; Cunningham, K. A.; Fone, K. C.; Gershon, M.; Di Giovanni, G.; Goodfellow, N. M.; Halberstadt, A. L.; Hartley, R. M.; Hassaine, G.; Herrick-Davis, K.; Hovius, R.; Lacivita, E.; Lambe, E. K.; Leopoldo, M.; Levy, F. O.; Lummis, S. C. R.; Marin, P.; Maroteaux, L.; McCreary, A. C.; Nelson, D. L.; Neumaier, J. F.; Newman-Tancredi, A.; Nury, H.; Roberts, A.; Roth, B. L.; Roumier, A.; Sanger, G. J.; Teitler, M.; Sharp, T.; Villalón, C. M.; Vogel, H.; Watts, S. W.; Hoyer D. International Union of Basic and Clinical Pharmacology. CX. Classification of Receptors for 5-hydroxytryptamine; Pharmacology and Function. *Pharmacol. Rev.* **2021**, *73*, 310–520.

8 Zweckstetter, M.; Dityatev, A.; Ponimaskin, E. Structure of Serotonin Receptors: Molecular Underpinning of Receptor Activation and Modulation. *Signal Transduct. Target Ther.* **2021**, *6*, 243.

- 9 Bhattachary, S.; Vaidehi, N. Computational Mapping of the Conformational Transitions in Agonist Selective Pathways of a G-Protein Coupled Receptor. *J. Am. Chem. Soc.* **2010**, *132*, 5205–5214.
- 10 Hu, X.; Wang, Y.; Hunkele, A.; Provasi, D.; Pasternak, G. W.; Filizola, M. Kinetic and Thermodynamic Insights into Sodium Ion Translocation Through the μ-opioid Receptor from Molecular Dynamics and Machine Learning Analysis. *PLOS Comput. Biol.* **2019**, *15*, e1006689.
- 11 Kohlhoff, K. J.; Shukla, D.; Lawrenz, M.; Bowman, G. R.; Konerding, D. E.; Belov, D.; Altman, R. B.; Pande, V. S. Cloud-Based Simulations on Google Exacycle Reveal Ligand Modulation of GPCR Activation Pathways. *Nature Chem.* **2014**, *6*, 15–21.
- 12 Li, J.; Jonsson, A. L.; Beuming, T.; Shelley, J. C.; Voth, G. A. Ligand-Dependent Activation and Deactivation of the Human Adenosine A_{2A} Receptor. *J. Am. Chem. Soc.* **2013**, *135*, 8749–8759.
- 13 Miao, Y.; McCammon, J. A. Graded Activation and Free Energy Landscapes of a Muscarinic G-Protein-Coupled Receptor. *Proc. Natl. Acad. Sci. U.S.A.* **2016**, *113*, 12162–12167.
- 14 Ibrahim, P.; Clark, T. Metadynamics Simulations of Ligand Binding to GPCRs. *Curr. Opin. Struct. Biol.* **2019**, *55*, 129–137.
- 15 Dror, R.; Arlow, D. H.; Maragakis, P.; Mildorf, T. J.; Pan, A. C.; Xu, H.; Borhani, D.; Shaw, D. Activation Mechanism of the β₂-Adrenergic Receptor. *Proc. Natl. Acad. Sci. U.S.A.* **2011**, *108*, 18684–18689.
- 16 Alhadeff, R.; Vorobyov, I.; Yoon, H. W.; Warshel, A. Exploring the Free-Energy Landscape of GPCR Activation. *Proc. Natl. Acad. Sci. U.S.A.* **2018**, *115*, 10327–10332.
- 17 Mondal, D.; Kolev, V.; Warshel, A. Exploring the Activation Pathway and Gi-Coupling Specificity of the μ-Opioid Receptor. *Proc. Natl. Acad. Sci. U.S.A.* **2020**, *117*, 26218–26225.
- 18 Yang, Y. I.; Shao, Q.; Zhang, J.; Yang, L.; Gao, Y. Q. Enhanced Sampling in Molecular Dynamics. *J. Chem. Phys.* **2019**, *151*, 070902.
- 19 Fleetwood, O.; Carlsson, J.; Delemotte, L. Identification of Ligand-Specific G Protein-Coupled Receptor States and Prediction of Downstream Efficacy via Data-Driven Modeling. *eLife* **2021**, *10*, e60715.

- 20 Fleetwood, O.; Matricon, P.; Carlsson, J.; Delemotte, L. Energy Landscapes Reveal Agonist Control of G Protein-Coupled Receptor Activation via Microswitches. *Biochem.* **2020**, *59*, 880–891.
- 21 Provasi, D.; Artacho, M. C.; Negri, A.; Mobarec, J. C.; Filizola, M. Ligand-Induced Modulation of the Free-Energy Landscape of G Protein-Coupled Receptors Explored by Adaptive Biasing Techniques. *PLOS Comput. Biol.* **2011**, *7*, e1002193.
- 22 Saleh, N.; Haensele, E.; Banting, L.; Sopkova-de Oliveira Santos, J.; Whitley, D. C.; Saldino, G.; Gervasio, F. L.; Bureau, R.; Clark, T. A Three-Site Mechanism for Agonist/Antagonist Action on the Vasopressin Receptors. *Angew. Chemie Int. Ed.*, **2016**, *128*, 8008–8012.
- 23 Laio, A.; Gervasio, F. L. Metadynamics: A Method to Simulate Rare Events and Reconstruct the Free Energy in Biophysics, Chemistry and Material Science. *Rep. Prog. Phys.* **2008**, *71*, 126601.
- 24 Bussi, G.; Laio, A. Using Metadynamics to Explore Complex Free-Energy Landscapes. *Nature Rev. Phys.* **2020**, *2*, 200–212.
- 25 Bussi, G.; Gervasio, F. L.; Laio, A.; Parrinello, M. Free-Energy Landscape for β Hairpin Folding from Combined Parallel Tempering and Metadynamics. *J. Am. Chem. Soc.* **2006**, *128*, 13435–13441.
- 26 Raiteri, P.; Laio, A.; Gervasio, F. L.; Micheletti, C.; Parrinello. M. Efficient Reconstruction of Complex Free Energy Landscapes by Multiple Walkers Metadynamics. *J. Phys. Chem. B* **2006**, 110, 3533–3539.
- 27 Mattedi, G.; Acosta-Gutiérrez, S.; Clark, T.; Gervasio, F. L. A Combined Activation Mechanism for the Glucagon Receptor. *Proc. Nat. Acad. Sci. U.S.A.* **2020**, *117*, 15414–15422.
- 28 Provasi, D.; Bortolato, A.; Filizola, M. Exploring Molecular Mechanisms of Ligand Recognition by Opioid Receptors with Metadynamics. *Biochemistry* **2009**, 48, 10020–10029.
- 29 Saleh, N.; Ibrahim, P.; Saladino, G.; Gervasio, F. L.; Clark, T. An efficient Metadynamics-Based Protocol to Model the Binding Affinity and the Transition State Ensemble of GPCR-Ligands. *J. Chem. Inf. Model.* **2017**, *57*, 1210–1217.

- 30 Ibrahim, P.; Wifling, D.; Clark, T. A Universal Activation Index for Class A GPCRs. *J. Chem. Inf. Model.* **2019**, *59*, 3938–3945.
- 31 Bonomi, M.; Braduardi, D.; Bussi, G.; Camilloni, C.; Provasi, D.; Raiteri, P.; Donadio, D.; Marinelli, F.; Pietrucci, F.; Broglie, R. A.; Parrinello, M. PLUMED: A Portable Plugin for Free Energy Calculations with Molecular Dynamics. *Comp. Phys. Comm.* **2009**, *180*, 1961–1972.
- 32 Tribello, G. A.; Bonomi, M.; Branduardi, D.; Camilloni, C.; Bussi, G. PLUMED2: New Feathers for an Old Bird. *Comp. Phys. Comm.* **2014**, *185*, 604–613.
- 33 Nicoli, A.; Haag, F.; Marcinek, P.; He, R.; Kreißl, J.; Stein, J.; Marchetto, A.; Dunkel, A.; Hofmann, T.; Krautwurst, D.; Di Pizio, A. Modeling the Orthosteric Binding Site of the G Protein-Coupled Odorant Receptor OR5K1. *J. Chem. Inf. Model.*, **2023**, ASAP article, DOI: 10.1021/acs.jcim.2c00752.
- 34 Benkel, T.; Zimmermann, M.; Zeiner, J.; Bravo, S.; Merten, V.; Lim, V. J. Y.; Matthees, E. S. F.; Drube, J.; Miess-Tanneberg, E.; Malan, D.; Szpakowska, M.; Monteleone, S.; Grimes, J.; Koszegi, Z.; Lanoiselée, Y.; O'Brien, S.; Pavlaki, N.; Dobberstein, N.; Inoue, A.; Nikolaev, V.; Calebiro, D.; Chevigné, A.; Sasse, P.; Schulz, S.; Hoffmann, C.; Kolb, P.; Waldhoer, M.; Simon, K.; Gomeza, J.; Kostenis, E. How Carvedilol activates β2-adrenoceptors. *Nature Commun.*, **2022**, *13*, 7109.
- 35 Kobilka, B. K.; Deupi, X. Conformational Complexity of G-Protein-Coupled Receptors. *Trends. Pharmacol. Sci.* **2007**, *28*, 397–406.
- 36 Nygaard, R.; Frimurer, T. M.; Holst, B.; Rosenkilde, M. M.; Schwartz, T. W. Ligand Binding and Micro-Switches in 7TM Receptor Structures. *Trends Pharmacol. Sci.* **2009**, *30*, 249–259.
- 37 De Deurwaerdère, P.; Bharatiya, R.; Chagraoui, A.; Di Giovanni, G. Constitutive Activity of 5-HT Receptors: Factual Analysis. *Neuropharmacology* **2020**, *168*, 107967.
- 38 Rasmussen, S. G. F.; DeVree, B. T.; Zou, Y.; Kruse, A. C.; Chung, K. Y.; Kobilka, T. S.; Thian, F. S.; Chae, P. S.; Pardon, E.; Calinski, D.; Mathiesen, J. M.; Shah, S. T. A.; Lyons, J. A.; Caffrey, M.; Gellman, S. H.; Steyaert, J.; Skiniotis, G.; Weis, W. I.; Sunahara, R. K.; Kobilka, B. K. Crystal Structure of the β₂ Adrenergic Receptor–Gs Protein Complex. *Nature* **2011**, 477, 549–555.

- 39 Zhou, Q.; Yang, D.; Wu, M.; Guo, Y.; Guo, W.; Zhong, L.; Cai, X.; Dai, A.; Jang, W.; Shakhnovich, E. I.; Liu, Z.-J.; Stevens, R. C.; Lambert, N. A.; Babu, M. M.; Wang, M.-W.; Zhao, S. Common activation mechanism of class A GPCRs. *eLife*, **2019**, https://doi.org/10.7554/eLife.50279
- 40 Bock, A.; Bermudez, M. Allosteric Coupling and Biased Agonism in G-Protein-Coupled Receptors. *FEBS* **2021**, *288*, 2513–2528.
- 41 Strader, C. D.; Sigal, I. S.; Candelore, M. R.; Rands, E.; Hill, W. S.; Dixon, R. A. F. Conserved Aspartic Acid Residues 79 and 113 of the Beta-Adrenergic Receptor Have Different Roles in Receptor Function. *J. Biol. Chem.* **1988**, *263*, 10267–10271.
- 42 Liegeois, J.-F.; Lespagnard, M.; Salas, E. M.; Mangin, F.; Scuvee-Moreau, J.; Dilly, S. Enhancing a CH-π Interaction to Increase the Affinity for 5-HT_{1A} Receptors. *ACS Med. Chem. Lett.*, **2014**, *5*, 358–362.
- 43 Ho, B. Y.; Karschin, A.; Branchek, T.; Davidson, N.; Lester, H. A. The Role of Conserved Aspartate and Serine Residues in Ligand Binding and in Function of the 5-HT_{1A} Receptor: A Site-Directed Mutation Study. *FEBS Lett.* **1992**, *12*, 259–262.
- 44 Strader, C. D.; Candelore, M. R.; Hill; W. S.; Sigal, I. S.; Dixon, R. A. F. Identification of Two Serine Residues Involved in Agonist Activation of the β-Adrenergic Receptor. *J. Biol. Chem.* **1989**, *264*, 13572–13578.
- 45 Katritch, V.; Reynolds, K. A.; Cherezov, V.; Hanson, M. A.; Roth, C. B.; Yeager, M.; Abagyan, R. Analysis of Full and Partial Agonists Binding to β₂-Adrenergic Receptor Suggests a Role of Transmembrane Helix V in Agonist-Specific Conformational Changes. *J. Mol. Recognit.* **2009**, *22*, 307–318.
- 46 Bywater, J. Location and Nature of the Residues Important for Ligand Recognition in G-Protein Coupled Receptors. *Mol. Recognit.* **2005**, *18*, 60–72.
- 47 Swaminath, G.; Xiang, Y.; Lee, T. W.; Steenhuis, J.; Parnot, C.; Kobilka, B. K. Sequential Binding of Agonists to the β₂ Adrenoceptor. Kinetic Evidence for Intermediate Conformational States. *J. Biol. Chem.* **2004**, *279*, 686–691.
- 48 Yuan, S.; Peng, Q.; Palczewski, K.; Vogel, H.; Filipek, S. Mechanistic Studies on the Stereoselectivity of the Serotonin 5-HT_{1A} Receptor. *Angew. Chem. Int. Ed.* **2016**, *55*, 8661–8665.

- 49 Sarkar, P.; Mozumder, S.; Bej, A.; Mukherjee, S.; Sengupta, J.; Chattopadhyay, A. Structure, Dynamics and Lipid Interactions of Serotonin Receptors: Excitements and Challenges. *Biophys. Rev.* **2021**, *13*, 101–122.
- 50 Imai, S.; Yokomizo, T.; Kofuku, Y.; Shiraishi, Y.; Ueda, T.; Shimada, I. Structural Equilibrium Underlying Ligand Dependent Activation of β₂-Adrenoreceptor. *Nat. Chem. Biol.* **2020**, *16*, 430–439.
- 51 Eddy, M. T.; Martin, B. T.; Wüthrich, K. A_{2A} Adenosine Receptor Partial Agonism Related to Structural Rearrangements in an Activation Microswitch. *Structure* **2021**, *29*, 170–176.
- 52 Grahl, A.; Abiko, L. A.; Isogai, S.; Sharoe, T.; Grzesiek, S. A High-Resolution Description of β₁-Adrenergic Receptor Functional Dynamics and Allosteric Coupling from Backbone NMR. *Nature Commun.* **2020**, *11*, 2216.
- 53 Abraham, M. J.; Murtola, T.; Schulz, R.; Páll, S.; Smith, J. C.; Hess, B.; Lindahl, E. GROMACS: High Performance Molecular Simulations Through Multi-Level Parallelism from Laptops to Supercomputers. *SoftwareX* **2015**, *1*–2, 19–25.
- 54 Bussi, G.; Donadio, D.; Parrinello, M. Canonical sampling through velocity rescaling. *J. Chem. Phys.*, **2007**, *126*, 014101.
- 55 Hess, B.; Bekker, H.; Berendsen, H. J. C.; Fraaije. J. G. E. M. LINCS: A Linear Constraint Solver for Molecular Simulations. *J. Comput. Chem.* **1997**, *18*, 1463–1472.
- 56 Darden, T.; York, D.; Pedersen, L. Particle Mesh Ewald: An N log (N) Method for Ewald Sums in Large Systems. *J. Chem. Phys.* **1993**, *98*, 10089–10092.
- 57 Berendsen, H. J. C.; Grigera, J. R.; Straatsma, T. P. The Missing Term in Effective Pair Potentials. *J. Phys. Chem.* **1987**, *91*, 6269–6271.
- 58 Barducci, A.; Bussi, G.; Parrinello, M. Well-Tempered Metadynamics: A Smoothly Converging and Tunable Free-Energy Method. *Phys. Rev. Lett.* **2008**, *100*, 020603.
- 59 Tiwary, P.; Parrinello, M. A Time-Independent Free Energy Estimator for Metadynamics. *J. Phys. Chem. B* **2015**, *119*, 736–742.
- 60 Case, D. A.; Ben-Shalom, I. Y.; Brozell, S. R.; Cerutti, D. S.; Cheatham, T. E.; Cruzeiro, V. W. D.; Darden, T. A.; Duke, R. E.; Ghoreishi. D.; Gilson, M. K.; Gohlke, H.; Goetz, A. W.; Greene, D.; Harris, R.; Homeyer, N.; Huang, Y.; Izadi, S.; Kovalenko, A.; Kurtzman,

T.; Lee, T. S.; LeGrand, S.; Li, P.; Lin, C.; Liu, J.; Luchko, T.; Luo, R.; Mermelstein, D. J.; Merz, K. M.; Miao, Y.; Monard, G.; Nguyen, C.; Nguyen, H.; Omelyan, I.; Onufriev, A.; Pan, F.; Qi, R.; Roe, D. R.; Roitberg, A.; Sagui, C.; Schott-Verdugo, S.; Shen, J.; Simmerling, C. L.; Smith, J.; Salomon-Ferrer, R.; Swails, J.; Walker, R. C.; Wang, J.; Wei, H.; Wolf, R. M.; Wu, X.; Xiao, L.; York, D. M.; Kollman, P. A. AMBER 2018.; University of California.; San Francisco.; **2018**.

61 Pettersen, E. F.; Goddard, T. D.; Huang, C. C.; Couch, G. S.; Greenblatt, D. M.; Meng, E: C.; Ferrin, T. E. UCSF Chimera - A Visualization System for Exploratory Research and Analysis. *J. Comput. Chem.* **2004**, *25*, 1605–1612.

62 Hunter, J. D. Matplotlib: A 2D Graphics Environment. Comput. Sci. Eng. 2007, 9, 90–95.

ToC Graphic

